IEEE Access
Multidisciplinary | Rapid Review | Open Access Journal

Received June 6, 2020, accepted July 1, 2020, date of publication July 6, 2020, date of current version July 20, 2020.

Digital Object Identifier 10.1109/ACCESS.2020.3007233

Dynamic Fractional Order Sliding Mode Control Method of Micro Gyroscope Using Double Feedback Fuzzy Neural Network

JUNTAO FEI, (Senior Member, IEEE), AND FANG CHEN
College of IoT Engineering, Hohai University, Changzhou 213022, China
Jiangsu Key Laboratory of Power Transmission and Distribution Equipment Technology, Changzhou 213022, China

Corresponding author: Juntao Fei (jtfei@hhu.edu.cn)

This work was supported in part by the National Science Foundation of China under Grant 61873085, and in part by the Natural Science Foundation of Jiangsu Province under Grant BK20171198.

ABSTRACT In this paper, a dynamic fractional order sliding mode control method based on a double feedback fuzzy neural network controller is proposed to deal with the unknown parameters and upper bound of uncertainty. Firstly, the switching function of the dynamic fractional order sliding mode control is designed, which not only fixes switching function of the ordinary sliding mode control, but also increases the fractional order, so that the switching function has a higher degree of freedom. In addition, the expert experience of fuzzy logic and the self-learning ability of neural network are used to improve the control accuracy and estimate the upper bound of uncertainty. Meanwhile, by using Lyapunov stability theory, the adaptive laws of unknown parameters in the system are derived to realize online adjustment, which increases the robustness of the system. Finally, the simulation results show that the proposed control method is more effective than the ordinary adaptive sliding mode control method in terms of convergence speed, parameter fitting effect, output signal tracking speed and tracking error.

INDEX TERMS Fractional order, dynamical sliding mode control, fuzzy system, neural network, micro gyroscope.

I. INTRODUCTION

Gyroscope is an angular motion detection device, which was first used in navigation. With the development of science and technology, the types of gyroscopes have increased, and the application fields have become more and more extensive, such as automobile safety, smartphone [1], aircraft, etc. With its own advantages, micro gyroscope has become one of the important directions for the future development of gyroscopes. Due to the limitation of the technology, its accuracy is far lower than that of traditional gyroscopes, and various control methods can be used to improve its accuracy and performance. In [2], by comparing the working state of the gyroscope with the reference model, the key system parameters can be estimated online using adaptive control method. In [3], a sliding mode control method based on system identification is presented to control autonomous aerial vehicles. Song *et al.* [4] presents a parameter-based sliding mode finite-time bounded control to study the mean square finite time bounded control of uncertain stochastic systems. Therefore, sliding mode control is used to improve the accuracy and unbiased tracking of output signals in micro gyroscopes with uncertainty and external disturbance. Fei and Feng [5] proposed an adaptive fuzzy super-twisting sliding mode control, to improves the performance of the system. In [6], Chen and Fei derived a fractional order adaptive sliding mode controller to estimate the unknown parameters in micro gyroscope.

The mathematical model of neurons in neural networks was first proposed by Mcculloch and Pitts in 1943. It has been widely used in image processing [7], load forecasting [8], medical device [9] and pattern recognition [10]. The greatest advantage of artificial neural networks is that the observed data is continuously learned as a mechanism for approaching arbitrary function. In order to improve the robustness of the single-link flexible manipulator control,

The associate editor coordinating the review of this manuscript and approving it for publication was Valentina E. Balas.

an adaptive neural approximator is used to compensate for the system uncertainty, and a sliding mode control method is designed to rapidly move the system joint to a predetermined position and suppress the vibration on the manipulator [11]. Saeed *et al.* [12] discusses the process of vehicle route decision making by using cognitive memory to store the route experience. It utilized the artificial neural networks to minimize the learning error rate and achieve the cognitive route decision. In [13], Qian and Fan proposes a terminal sliding mode control method to control the load frequency of renewable energy power generation system, and designes radial basis function neural networks to approximate the entire uncertainty of the system. In [14], a new robust backstepping sliding mode controller for twelve-rotator UVA based on self-recurrent wavelet neural network is proposed to estimate the lumped uncertainty, improve the accuracy, and enhance the robustness. Novel adaptive neural network controllers are proposed for a class of dynamic system and active power filters in [15]–[18].

Because the discontinuity of the reaching law in the ordinary sliding mode control is transferred directly to the control, which causes system chattering. The first-order dynamic sliding mode control corrects the switching function of the ordinary sliding mode control. The modified switching function is not only related to the system state, but also to the system control input. It transfers the discontinuities to the first derivative of the control and reduces the chattering. In [19], a global dynamic sliding mode control method is presented to meet the high-performance requirement of PMSM speed servo system for non-sinusoidal oscillation control system of continuous casting crystallizer. In [20], Fethalla *et al.* proposed a closed-loop system consisting of dynamic sliding mode controller and backstepping controller, which is combined with a nonlinear disturbance observer to track the attitude trajectory of a quadrotor UAV. In [21], [22], a dynamic sliding mode controller with integral switching gain and an adaptive neural dynamic terminal sliding mode controller is presented to approximate the harmonic compensation performance of APF. In [23], an intelligent dynamic sliding mode control method based on field programmable gate array is presented, and recurrent wavelet neural network estimator is used to control the motion position of linear ultrasonic motor. When designing a sliding mode controller, the advantages of fractional calculus algorithm can be utilized to ensure the fast response of the closed-loop system in the presence of disturbances. The method combining fractional-order calculus algorithm with sliding mode control is used in satellite systems [24] and permanent magnet synchronous motor [25], [26]. In [27], [28] by adding fractional order on the nonsingular terminal sliding surface, fuzzy neural controllers are proposed to enhance the tracking accuracy of the control system.

Based on the discussion of the advantages of the above methods, this paper proposes a neural network dynamic sliding mode control method based on fractional calculus for micro gyroscope. The specific contributions are summarized as:

(1) After modifying the switching function of the ordinary sliding mode control, the switching function of the dynamic fractional order sliding mode control is obtained and the discontinuous term in the reaching law is transferred to the derivative of the control, which effectively reduce the chattering. Meanwhile, the fractional order term is added to the modified switching function to enhance the continuity of the sliding mode control and improve the convergence speed of the system.

(2) Combining fuzzy system and neural network, and introducing recursive links inside and outside the fuzzy neural network to constitute a double feedback fuzzy neural network, which solves the problem that the parameters in the fuzzy system rule set and membership function can only be selected by experience. Adjusting weight learning and induction learning are carried out at the same time, with the dynamic mapping ability, which improves the disturbance rejection ability and generalization ability of the system.

(3) In the case of unknown parameters in the system and the fuzzy neural network, the Lyapunov stability theory in adaptive control is used to derive an adaptive law to estimate unknown parameter values, which is robust to parameter changes and disturbances, and can better realize the system output signals tracking without deviation.

The rest of this paper is as follows. The second part is the analysis and modification of the micro gyroscope's dynamics model. The section III is the design of dynamic fractional order sliding mode control. In the fourth part, the double feedback fuzzy neural network is designed to estimate the lumped uncertainty of the system. Then, the dynamic fractional order sliding mode control method using double feedback fuzzy neural network is designed. In the sixth part, the proposed method is simulated to verify the feasibility. The section VII is the summary of the paper.

II. GYNAMICS ANALYSIS OF MICRO GYROSCOPE

In order to analyze the dynamic model of micro gyroscope, firstly, the rotation coordinate axis is set up, and the x-axis is the driving vibration direction, the y-axis is the direction for detecting vibration, and the z-axis is the direction of the system input angular velocity. Fig.1 is the schematic diagram of micro gyroscope structure.

Considering the influence of structure error, the basic dynamic equation of micro gyroscope is as follows:

$$m\ddot{x} + d_{xx}\dot{x} + d_{xy}\dot{y} + k_{xx}x + k_{xy}y = u_x + 2m\Omega_z\dot{y} \quad (1)$$

$$m\ddot{y} + d_{xy}\dot{x} + d_{yy}\dot{y} + k_{xy}x + k_{yy}y = u_y - 2m\Omega_z\dot{x} \quad (2)$$

where d_{xx}, d_{yy} and d_{xy} are driving direction, detecting direction and coupling damping coefficient respectively, k_{xx}, k_{yy} and k_{xy} are driving direction, detecting direction and coupling stiffness coefficient respectively, Ω_z is the system input angular velocity, m is the mass of mass block, u_x and u_y are control inputs.

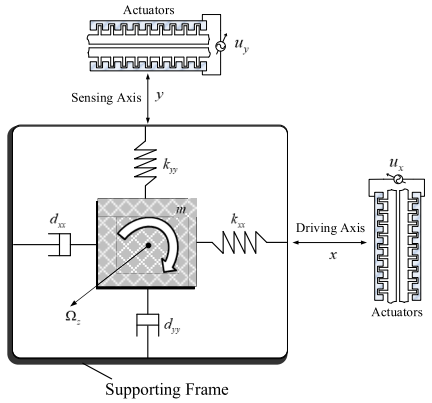

FIGURE 1. Schematic diagram of micro gyroscope structure.

The dimensionless dynamic model is obtained by dividing the two sides of equation (1)-(2) by mass block m, natural resonance frequency squared ω_0^2 and reference length q_0. The expression is as follows:

$$\ddot{x}^* + d_{xx}^*\dot{x}^* + d_{xy}^*\dot{y}^* + \omega_{xx}x^* + \omega_{xy}y^* = u_x^* + 2\Omega_z^*\dot{y}^* \quad (3)$$

$$\ddot{y}^* + d_{xy}^*\dot{x}^* + d_{yy}^*\dot{y}^* + \omega_{xy}x^* + \omega_{yy}y^* = u_y^* - 2\Omega_z^*\dot{x}^* \quad (4)$$

where $x^* = \frac{x}{q_0}, y^* = \frac{y}{q_0}, d_{xx}^* = \frac{d_{xx}}{m\omega_0}, d_{xy}^* = \frac{d_{xy}}{m\omega_0}, d_{yy}^* = \frac{d_{yy}}{m\omega_0}, \omega_{xx}^* = \frac{k_{xx}}{m\omega_0^2}, \omega_{xy}^* = \frac{k_{xy}}{m\omega_0^2}, \omega_{yy}^* = \frac{k_{yy}}{m\omega_0^2}, u_x^* = \frac{u_x}{m\omega_0^2 q_0}, u_y^* = \frac{u_y}{m\omega_0^2 q_0}, \Omega_z^* = \frac{\Omega_z}{\omega_0}$.

The (3) and (4) is rewritten in vector form as follows:

$$\ddot{q} + D\dot{q} + Kq = u - 2\Omega\dot{q} \quad (5)$$

where $q = \begin{bmatrix} x^* \\ y^* \end{bmatrix}, D = \begin{bmatrix} d_{xx}^* & d_{xy}^* \\ d_{xy}^* & d_{yy}^* \end{bmatrix}, K = \begin{bmatrix} \omega_{xx}^* & \omega_{xy}^* \\ \omega_{xy}^* & \omega_{yy}^* \end{bmatrix}, u = \begin{bmatrix} u_x^* \\ u_y^* \end{bmatrix}, \Omega = \begin{bmatrix} 0 & -\Omega_z^* \\ \Omega_z^* & 0 \end{bmatrix}$.

Considering the parameters uncertainty and external disturbance, the Eq. (5) can be expressed as:

$$\ddot{q} + (D + 2\Omega + \Delta D)\dot{q} + (K + \Delta K)\, q = u + d \quad (6)$$

where ΔD and ΔK are the uncertainty of $D + 2\Omega$ and K, respectively; d is an external disturbance. Let $\psi = -(D_d + 2\Omega)\,\dot{q} - Kq, f_g = d - \Delta D\dot{q} - \Delta Kq$, the micro gyroscope system mode can be rewritten as:

$$\ddot{q} = \psi + u + f_g \quad (7)$$

Because of the demand of dynamic sliding mode design in the next part, the derivative of the system model needs to be calculated. The derivative of the mathematical model is as follows:

$$\dddot{q} = \dot{\psi} + \dot{u} + \dot{f}_g \quad (8)$$

We assume that the upper bound of f_g is F_{d_1}, satisfying $|f_g| \le F_{d_1}$ and the upper bound of $\dot{f}_g$ is F_{d_2}, satisfying $|\dot{f}_g| \le F_{d_2}$, where F_{d_1} and F_{d_2} are positive constants.

III. DYNAMIC FRACTIONAL ORDER SLIDING MODE CONTROLLER

First, the ordinary sliding surface is designed as:

$$s = ce + \dot{e} \quad (9)$$

where e is a tracking error, $e = q - q_r$, c is a positive constant, q_r is a reference trajectory.

The derivative of Eq. (9) is as:

$$\dot{s} = c\dot{e} + \ddot{e} \quad (10)$$

According to the ordinary sliding surface, the dynamic fractional order switching function is constructed as follows:

$$\begin{aligned} \sigma &= \dot{s} + \lambda_1 s + \lambda_2 D^{\alpha-1} e \\ &= \ddot{e} + (c + \lambda_1)\,\dot{e} + \lambda_1 c e + \lambda_2 D^{\alpha-1} e \end{aligned} \quad (11)$$

where λ_1 is a dynamic sliding surface parameter and λ_2 is a fractional order parameter, which are the positive constants.

The fractional order operation mainly includes the definition of Caputo fractional order calculus, Grunwald-Letnikov fractional order calculus and Riemann-Lionville fractional order calculus. The fractional order operation in (11) is the definition of Caputo fractional order differential. Its expression is ${}_{t_0}D_t^{\alpha} f(t) = \frac{1}{\Gamma(m-\alpha)} \int_{t_0}^{t} \frac{f^{(m)}(t)}{(t-\tau)^{\alpha-m+1}} d\tau$. For the convenience of expression, ${}_{t_0}D_t^{\alpha}$ is abbreviated to D^{α} in the paper.

When $\sigma = 0$, according to the stability of fractional order system, we can get that $\dot{s} + \lambda_1 s + \lambda_2 D^{\alpha-1} e = 0$ is a gradually stable dynamic system [29], [30].

Differentiating (11) and substituting (7)-(8) and (10) into the derivative of (11) get:

$$\begin{aligned} \dot{\sigma} &= \ddot{s} + \lambda_1 \dot{s} + \lambda_2 D^{\alpha} e \\ &= \dddot{e} + (c + \lambda_1)\,\ddot{e} + \lambda_1 c\dot{e} + \lambda_2 D^{\alpha} e \\ &= \left(\ddot{q} - \ddot{q}_r\right) + (c + \lambda_1)\left(\dot{q} - \dot{q}_r\right) + \lambda_1 c\dot{e} + \lambda_2 D^{\alpha} e \\ &= \left(\dot{\psi} + \dot{u} + \dot{f}_g - \ddot{q}_r\right) + (c + \lambda_1)\left(\psi + u + f_g - \dot{q}_r\right) \\ &\quad + \lambda_1 c\dot{e} + \lambda_2 D^{\alpha} e \end{aligned} \quad (12)$$

The dynamic fractional order equivalent control law is obtained:

$$\begin{aligned} u_{eq} = -\frac{1}{c + \lambda_1}\Big[&\dot{\psi} + \dot{u}_{eq} - \ddot{q}_r + (c + \lambda_1)\,\psi - (c + \lambda_1)\,\dot{q}_r \\ &+ \lambda_1 c\dot{e} + \lambda_2 D^{\alpha} e\Big] \end{aligned} \quad (13)$$

Then a switching controller is designed as:

$$u_{sw} = -\rho \frac{1}{c + \lambda_1} \frac{s}{\|s\|} \quad (14)$$

where ρ is the coefficient of switching term, which is an unknown parameter.

Thus, the control law u is designed as:

$$\begin{aligned} u = -\frac{1}{c + \lambda_1}\Big[&\dot{\psi} + \dot{u} - \ddot{q}_r + (c + \lambda_1)\,\psi - (c + \lambda_1)\,\dot{q}_r \\ &+ \lambda_1 c\dot{e} + \lambda_2 D^{\alpha} e + \rho \frac{s}{\|s\|}\Big] \end{aligned} \quad (15)$$

Lyapunov stability criterion: Consider a function $V : R^n \to R$ such that: $V(x) = 0$ if and only if $x = 0$; $V(x) > 0$

if and only if $x \neq 0$; $\dot{V}(x) = \frac{d}{dt}V(x) = \sum_{i=1}^{n} \frac{\partial V}{\partial x_i} f_i(x) = \nabla V \cdot f(x) \leq 0$ for all values of $x \neq 0$. Then $V(x)$ is called a Lyapunov function and the system is stable in the sense of Lyapunov.

To prove the stability of the system, design the Lyapunov function as:

$$V_1 = \frac{1}{2}\sigma^T\sigma \tag{16}$$

Then, making derivative of the Lyapunov function gives:

$$\begin{aligned}\dot{V}_1 &= \sigma^T\dot{\sigma} \\ &= \sigma^T\left[\left(\dot{\psi}+\dot{u}+\dot{f}_g-\dddot{q}_r\right)+(c+\lambda_1)\left(\psi+u+f_g-\ddot{q}_r\right)\right. \\ &\quad \left.+\lambda_1 c\dot{e}+\lambda_2 D^{\alpha}e\right] \\ &= \sigma^T\left[\dot{f}_g+(c+\lambda_1)f_g-\rho\frac{\sigma}{\|\sigma\|}\right] \\ &\leq \|\sigma\|\left[\dot{f}_g+(c+\lambda_1)f_g-\rho\right] \\ &\leq -\|\sigma\|\left[\rho-F_{d_2}-(c+\lambda_1)F_{d_1}\right] \end{aligned} \tag{17}$$

When $\rho \geq F_{d_2} + (c+\lambda_1)F_{d_1}$ is satisfied, $\dot{V}_1 \leq 0$ is guaranteed, that is, $\dot{V}_1$ is semi-negative definite, which can proves the asymptotically stability of the system.

IV. DESIGND OF DOUBLE FEEDBACK FUZZY NEURAL NETWORK

In the actual micro gyroscope system, the upper bound of the lumped uncertainty in the system cannot be measured, it is impossible to obtain the accurate switching term coefficient ρ, which results in the control law u designed in the third part cannot be used. Therefore, a fuzzy neural network is used to approximate the switching term coefficient, and the true value is replaced by the estimated value, which is used as the gain of the switching term.

In practice, the input of neural network is affected by complex factors such as operation, data preprocessing, resulting in deviation. Using the self-learning and self-organizing ability of the neural network and the fuzzy logic to express expert experience, the combination of neural network and fuzzy system can solve the problem that the parameters of fuzzy system rule set and membership function can only be selected by experience. The fuzzy system can modify the membership function and fuzzy rules in the continuous learning by adjusting the weight learning and inductive learning, and can ignore the fuzziness in the reasoning process of the fuzzy system. Hence, the combined system has the abilities of self-learning and process quantitative data, which improve the disturbance rejection ability and prediction accuracy.

For practical work, fuzzy neural network can solve static problems, but it is not suitable for micro gyroscope system with dynamic characteristics. In order to solve this problem, a double feedback fuzzy neural network is constructed by adding recursive links to the fuzzy network, which has the capacity of dynamic mapping, enhances the dynamic approximation ability of the network, has the ability to filter and suppress noise. In the learning process, while forming the fuzzy rules, the membership function is optimized to further optimize the network structure and improve the generalization ability and robustness.

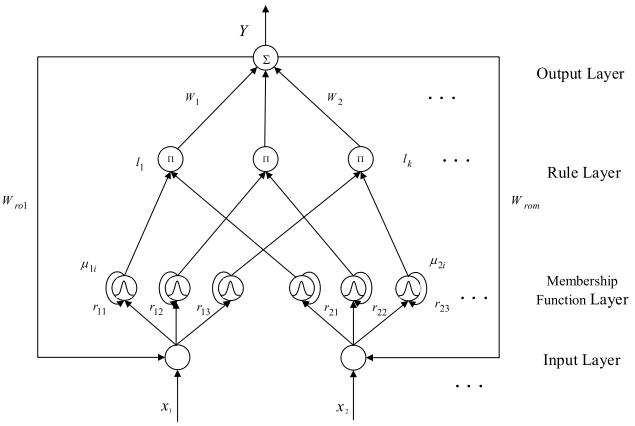

FIGURE 2. Neural network structural diagram.

The double feedback fuzzy neural network proposed in this paper is a four-layer neural network with two-layer closed-loop dynamic feedback and fuzzy system. It mainly includes input layer, membership function layer, rule layer and output layer. The structure is shown in Figure 2. The input of neural network is $\begin{bmatrix} q & \dot{q} \end{bmatrix}^T$ and the output is the upper bound estimate $\hat{\rho}$ of the lumped uncertainty in the micro gyroscope.

Layer 1: Input Layer

The input signal is $X = [x_1, x_2, \cdots, x_k]^T \in R^{k\times 1}$. Each node is directly connected with each component x_k of the input vector. The output signal of the output layer is exY, and the output layer is connected with the input layer by the outer layer weight W_{ro}. The output of each node is described as:

$$\theta_k = x_k \cdot W_{rok} \cdot exY \tag{18}$$

where $W_{ro} = [W_{ro1}, W_{ro2}, \cdots, W_{rok}]^T \in R^{k\times 1}$, $\theta = [\theta_1, \theta_2, \cdots, \theta_k]^T \in R^{k\times 1}$.

Layer 2: Membership Function Layer

Each node in this layer represents a membership function, which is represented by a Gaussian function. The center vector is

$c = [c_{11}, c_{12}, \cdots, c_{1m}, c_{21}, c_{22}, \cdots, c_{2m}, \cdots, c_{k1}, c_{k2}, \cdots, c_{km}]^T \in R^{num\times 1}$, for $num = k \times m$, the base width is

$b = [b_{11}, b_{12}, \cdots, b_{1m}, b_{21}, b_{22}, \cdots, b_{2m}, \cdots, b_{k1}, b_{k2}, \cdots, b_{km}]^T \in R^{num\times 1}$, and the feedback connection weight of the inner regression fuzzy neural network is

$r = [r_{11}, r_{12}, \cdots, r_{1m}, r_{21}, r_{22}, \cdots, r_{2m}, \cdots, r_{k1}, r_{k2}, \cdots, b_{km}]^T \in R^{num\times 1}$. Let the output of this layer is $\mu = [\mu_{11}, \mu_{12}, \cdots, \mu_{1m}, \mu_{21}, \mu_{22}, \cdots, \mu_{2m}, \cdots, \mu_{k1}, \mu_{k2}, \cdots, \mu_{km}]^T$, $\mu \in R^{num\times 1}$, that is:

$$\mu_{ki} = \exp\left[-\frac{\|\theta_k + r_{ki} \cdot ex\mu_{ki} - c_{ki}\|^2}{b_{ki}^2}\right], \quad for\ i = 1, 2, \ldots, m \tag{19}$$

where the layer feedback signal is defined as $ex\mu_{ki}$, μ_{ki} represents the i-th membership function of x_k.

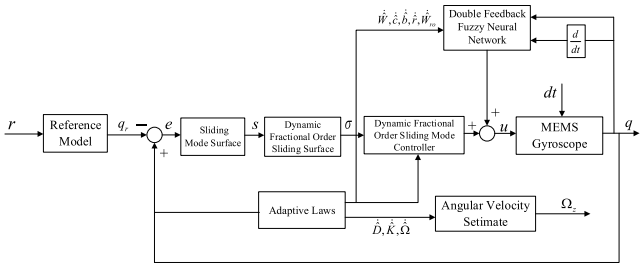

FIGURE 3. Controller block diagram.

Layer 3: Rule layer

The output of each node in the layer is the product of all the input signals of that node, namely:

$$l_j = \prod_{k=1}^{2} \mu_{kj}, \quad for\ j = 1, 2, \ldots, m \tag{20}$$

where $l = [l_1, l_2, \cdots, l_m]^T \in R^{m\times 1}$.

Layer 4: Output Layer

The neurons in this layer are connected to the neurons in the rule layer by the weight $W = [W_1, W_2, \cdots, W_m]^T \in R^{m\times 1}$. The output is the sum of all the input signals in this layer and the output signal is fed back to the neurons in the input layer through the outer layer gain. The output Y is expressed as:

$$Y = W^T l = W_1 l_1 + W_2 l_2 + \cdots + W_m l_m \tag{21}$$

V. DESIGN OF DYNAMIC FRACTIONAL ORDER SLIDING MODE CONTROLLER WITH DOUBLE FEEDBACK FUZZY NEURAL NETWORK

Using the neural network designed in the previous section, the upper bound of the lumped uncertainty of the system is approximated:

$$\hat{\rho} = \hat{W}^T \hat{l} \tag{22}$$

where the input of the neural network is $x = \begin{bmatrix} q & \dot{q} \end{bmatrix}^T$, q and $\dot{q}$ are the measurable signals in the system, $\hat{W}$ is the estimated value of the fuzzy neural network weight, and $\hat{l}$ is the function about x, $\hat{c}$, $\hat{b}$, $\hat{r}$, $\hat{W}_{ro}$. The neural network is used to adaptively learn the upper bound of the lumped uncertainty of the micro gyroscope. The parameters of the center vector, the base width vector, and the weight of the membership function in the neural network are adjusted automatically according to the designed adaptive law and updated in real time online.

Consequently, true value is replaced by the estimated value and the dynamic fractional order sliding mode control law with double feedback fuzzy neural network u' is expressed as:

$$u' = -\frac{1}{c+\lambda_1}\left[\dot{\psi} + \dot{u}' - \dddot{q}_r + (c+\lambda_1)\psi - (c+\lambda_1)\ddot{q}_r + \lambda_1 c\dot{e} + \lambda_2 D^{\alpha} e + \hat{\rho}\frac{s}{\|s\|}\right] \tag{23}$$

In order to design an adaptive law for unknown parameters in the system, adaptive laws for unknown parameter estimates $\hat{D}$, $\hat{K}$, $\hat{\Omega}$, $\hat{W}$, $\hat{c}$, $\hat{b}$, $\hat{r}$ and $\hat{W}_{ro}$ are designed using Lyapunov stability theory instead of their own unknown true values. Adaptive control enables the system output signal to better track the output response of the reference model. The designed adaptive law is independent of the object parameters, easy to implement, has good dynamic characteristics and disturbance rejection ability.

There are optimal neural network weight, optimal center vector c^*, optimal base width b^*, optimal inner feedback weight r^* and optimal outer feedback weight W_{ro}^*, we can get the bound of lumped uncertainty $\rho = W^{*T} l^* + \varepsilon$, where ε is the mapping error, and define the estimated error of the parameter as:

$$\begin{aligned} \tilde{D} &= \hat{D} - D^* \ \tilde{K} = \hat{K} - K^* \ \tilde{\Omega} = \hat{\Omega} - \Omega^* \\ \tilde{W} &= \hat{W} - W^* \ \tilde{c} = \hat{c} - c^* \ \tilde{b} = \hat{b} - b^* \\ \tilde{r} &= \hat{r} - r^* \ \tilde{W}_{ro} = \hat{W}_{ro} - W_{ro}^* \ \tilde{l} = \hat{l} - l^* \end{aligned} \tag{24}$$

And:

$$\begin{aligned} \dot{\tilde{D}} &= \dot{\hat{D}} \ \dot{\tilde{K}} = \dot{\hat{K}} \ \dot{\tilde{\Omega}} = \dot{\hat{\Omega}} \\ \dot{\tilde{W}} &= \dot{\hat{W}} \ \dot{\tilde{c}} = \dot{\hat{c}} \ \dot{\tilde{b}} = \dot{\hat{b}} \\ \dot{\tilde{r}} &= \dot{\hat{r}} \ \dot{\tilde{W}}_{ro} = \dot{\hat{W}}_{ro} \ \dot{\tilde{l}} = \dot{\hat{l}} \end{aligned} \tag{25}$$

The deviation between the true value and the estimated value of the upper bound of the uncertainty is calculated as:

$$\begin{aligned} \tilde{\rho} &= \rho - \hat{\rho} \\ &= W^{*T} l^* - \hat{W}^T \hat{l} + \varepsilon \\ &= \tilde{W}^T \hat{l} + \hat{W}^T \tilde{l} + \tilde{W}^T \tilde{l} + \varepsilon \end{aligned} \tag{26}$$

Taylor expansion of the rule layer output signal $\tilde{l}$ yields:

$$\begin{aligned} \tilde{l} = & \left.\frac{\partial l}{\partial c}\right|_{c=c^*} (c^* - \hat{c}) + \left.\frac{\partial l}{\partial b}\right|_{b=b^*} \left(b^* - \hat{b}\right) \\ & + \left.\frac{\partial l}{\partial r}\right|_{r=r^*} \left(r^* - \hat{r}\right) \\ & + \left.\frac{\partial l}{\partial W_{ro}}\right|_{W_{ro}=W_{ro}^*} \left(W_{ro}^* - \hat{W}_{ro}\right) + \Delta \\ = & \ l_c \cdot \tilde{c} + l_b \cdot \tilde{b} + l_r \cdot \tilde{r} + l_{W_{ro}} \cdot \tilde{W}_{ro} + \Delta \end{aligned} \tag{27}$$

where $l \in R^{5\times 1}$, $l_c = \begin{bmatrix} \frac{\partial l_1}{\partial c^T} \\ \frac{\partial l_2}{\partial c^T} \\ \vdots \\ \frac{\partial l_k}{\partial c^T} \end{bmatrix} = \begin{bmatrix} \frac{\partial l_1}{\partial c_1} & \frac{\partial l_1}{\partial c_2} & \cdots & \frac{\partial l_1}{\partial c_i} \\ \frac{\partial l_2}{\partial c_1} & \frac{\partial l_2}{\partial c_2} & \cdots & \frac{\partial l_2}{\partial c_i} \\ \vdots & \vdots & \ddots & \vdots \\ \frac{\partial l_k}{\partial c_1} & \frac{\partial l_k}{\partial c_2} & \cdots & \frac{\partial l_k}{\partial c_i} \end{bmatrix}_{k\times m\cdot i}$,

$l_b = \begin{bmatrix} \frac{\partial l_1}{\partial b^T} \\ \frac{\partial l_2}{\partial b^T} \\ \vdots \\ \frac{\partial l_k}{\partial b^T} \end{bmatrix} = \begin{bmatrix} \frac{\partial l_1}{\partial b_1} & \frac{\partial l_1}{\partial b_2} & \cdots & \frac{\partial l_1}{\partial b_i} \\ \frac{\partial l_2}{\partial b_1} & \frac{\partial l_2}{\partial b_2} & \cdots & \frac{\partial l_2}{\partial b_i} \\ \vdots & \vdots & \ddots & \vdots \\ \frac{\partial l_k}{\partial b_1} & \frac{\partial l_k}{\partial b_2} & \cdots & \frac{\partial l_k}{\partial b_i} \end{bmatrix}_{k\times m\cdot i}$, $l_r =$

$$\begin{bmatrix} \frac{\partial l_1}{\partial r^T} \\ \frac{\partial l_2}{\partial r^T} \\ \vdots \\ \frac{\partial l_k}{\partial r^T} \end{bmatrix} = \begin{bmatrix} \frac{\partial l_1}{\partial r_1} & \frac{\partial l_1}{\partial r_2} & \cdots & \frac{\partial l_1}{\partial r_i} \\ \frac{\partial l_2}{\partial r_1} & \frac{\partial l_2}{\partial r_2} & \cdots & \frac{\partial l_2}{\partial r_i} \\ \vdots & \vdots & \ddots & \vdots \\ \frac{\partial l_k}{\partial r_1} & \frac{\partial l_k}{\partial r_2} & \cdots & \frac{\partial l_k}{\partial r_i} \end{bmatrix}_{k\times m\cdot i}, \text{ and } l_{W_{ro}} = \begin{bmatrix} \frac{\partial l_1}{\partial W_{ro}^T} \\ \frac{\partial l_2}{\partial W_{ro}^T} \\ \vdots \\ \frac{\partial l_k}{\partial W_{ro}^T} \end{bmatrix} = \begin{bmatrix} \frac{\partial l_1}{W_{ro1}} & \frac{\partial l_1}{\partial W_{ro2}} & \cdots & \frac{\partial l_1}{\partial W_{roi}} \\ \frac{\partial l_2}{\partial W_{ro1}} & \frac{\partial l_2}{\partial W_{ro2}} & \cdots & \frac{\partial l_2}{\partial W_{roi}} \\ \vdots & \vdots & \ddots & \vdots \\ \frac{\partial l_k}{\partial W_{ro1}} & \frac{\partial l_k}{\partial W_{ro2}} & \cdots & \frac{\partial l_k}{\partial W_{roi}} \end{bmatrix}_{k\times m\cdot i}$$

Then (28) is rewritten as:

$$\tilde{\rho} = \tilde{W}^T\hat{l} + \hat{W}^T\left(l_c\cdot\tilde{c} + l_b\cdot\tilde{b} + l_r\cdot\tilde{r} + l_{W_{ro}}\cdot\tilde{W}_{ro}\right) + \varepsilon_0 \tag{28}$$

where the approximation error is defined as $\varepsilon_0 = \tilde{W}^T\tilde{l} + \varepsilon + \Delta$.

By substituting (24) into (23), the estimated control law u'' is:

$$u'' = -\frac{1}{c+\lambda_1}\left[\dot{\hat{\psi}} + \dot{u}'' - \dddot{q}_r + (c+\lambda_1)\,\ddot{\hat{\psi}} - (c+\lambda_1)\,\dddot{q}_r + \lambda_1 c\ddot{e} + \lambda_2 D^\alpha \ddot{e} + \hat{\rho}\frac{s}{\|s\|}\right] \tag{29}$$

where $\hat{\psi} = -\left(\hat{D} + 2\hat{\Omega}\right)\dot{q} - \hat{K}q$,

$\dot{\hat{\psi}} = -\left(\dot{\hat{D}} + 2\dot{\hat{\Omega}}\right)\dot{q} - \dot{\hat{K}}q - \left(\hat{D} + 2\hat{\Omega}\right)\ddot{q} - \hat{K}\dot{q}$ and u'' is adaptive dynamic fractional order sliding mode control law with double feedback fuzzy neural network.

The dynamic fractional order switching function (11) and the first derivative of the dynamic fractional order switching function (12) can be modified to:

$$\begin{cases} \sigma' = \left(\psi + u'' + f_g - \ddot{q}_r\right) + (c+\lambda_1)\,\ddot{e} + \lambda_1 c\dot{e} + \lambda_2 D^{\alpha-1}\ddot{e} \\ \dot{\sigma}' = \left(\dot{\psi} + \dot{u}'' + \dot{f}_g - \dddot{q}_r\right) + (c+\lambda_1)\left(\psi + u'' + f_g - \ddot{q}_r\right) \\ \quad + \lambda_1 c\ddot{e} + \lambda_2 D^\alpha \dot{e} \end{cases} \tag{30}$$

Design a new Lyapunov function:

$$\begin{aligned} V_2 = {} & \frac{1}{2}\sigma'^T\sigma' + \frac{1}{2}tr\left\{\tilde{D}M^{-1}\tilde{D}^T\right\} \\ & + \frac{1}{2}tr\left\{\tilde{K}N^{-1}\tilde{K}^T\right\} + \frac{1}{2}tr\left\{\tilde{\Omega}P^{-1}\tilde{\Omega}^T\right\} \\ & + \frac{1}{2\eta_1}\tilde{W}^T\tilde{W} + \frac{1}{2\eta_2}\tilde{c}^T\tilde{c} + \frac{1}{2\eta_3}\tilde{b}^T\tilde{b} \\ & + \frac{1}{2\eta_4}\tilde{r}^T\tilde{r} + \frac{1}{2\eta_5}\tilde{W}_{ro}^T\tilde{W}_{ro} \end{aligned} \tag{31}$$

where $M^T = M > 0, N^T = N > 0, P^T = P > 0$; $\eta_1, \eta_2, \eta_3, \eta_4$ and η_5 are the neural networks learning rates and they are all positive constants.

Let:

$$\begin{aligned} \zeta = {} & \frac{1}{2}tr\left\{\tilde{D}M^{-1}\tilde{D}^T\right\} + \frac{1}{2}tr\left\{\tilde{K}N^{-1}\tilde{K}^T\right\} + \frac{1}{2}tr\left\{\tilde{\Omega}P^{-1}\tilde{\Omega}^T\right\} \\ & + \frac{1}{2\eta_1}\tilde{W}^T\tilde{W} + \frac{1}{2\eta_2}\tilde{c}^T\tilde{c} + \frac{1}{2\eta_3}\tilde{b}^T\tilde{b} \\ & + \frac{1}{2\eta_4}\tilde{r}^T\tilde{r} + \frac{1}{2\eta_5}\tilde{W}_{ro}^T\tilde{W}_{ro} \end{aligned} \tag{32}$$

Substituting (30) into the derivative of (31) obtains:

$$\begin{aligned} \dot{V}_2 = {} & \sigma'^T\left[\left(\dot{\psi} + \dot{u}'' + \dot{f}_g - \dddot{q}_r\right) + (c+\lambda_1)\left(\psi + u'' + f_g - \ddot{q}_r\right) \right. \\ & \left. + \lambda_1 c\ddot{e} + \lambda_2 D^\alpha \dot{e}\right] + \dot{\zeta} \\ = {} & \sigma'^T\left[\dot{f}_g + (c+\lambda_1)f_g + \dot{\psi} + (c+\lambda_1)\,\psi - \dot{\hat{\psi}}\right. \\ & \left. - (c+\lambda_1)\,\hat{\psi}\right] - \hat{\rho}\frac{\sigma}{\|\sigma\|}\Bigg] + \dot{\zeta} \\ \le {} & \sigma'^T\left[\dot{f}_g + (c+\lambda_1)f_g + \dot{\psi} + (c+\lambda_1)\,\psi \right. \\ & \left. - \dot{\hat{\psi}} - (c+\lambda_1)\,\hat{\psi}\right] \\ & - \|\sigma'\|\left[\hat{W}^T\hat{l} - \rho + \rho\right] + \dot{\zeta} \\ = {} & \sigma'^T\left[\dot{f}_g + (c+\lambda_1)f_g + \dot{\psi} + (c+\lambda_1)\,\psi \right. \\ & \left. - \dot{\hat{\psi}} - (c+\lambda_1)\,\hat{\psi} - \rho\right] \\ & + \|\sigma'\|\left(\tilde{W}^T\hat{l} + \hat{W}^T\tilde{l} + \tilde{W}^T\tilde{l} + \varepsilon\right) + \dot{\zeta} \end{aligned} \tag{33}$$

Substituting (28) into (33) yields:

$$\begin{aligned} \dot{V}_2 \le {} & \sigma'^T\left[\dot{f}_g + (c+\lambda_1)f_g - \dot{\tilde{\psi}} - (c+\lambda_1)\,\tilde{\psi} - \rho\right] \\ & + \|\sigma'\|\left[\tilde{W}^T\hat{l}\hat{W}^T\left(l_c\cdot\tilde{c} + l_b\cdot\tilde{b} \right.\right. \\ & \left.\left. + l_r\cdot\tilde{r} + l_{W_{ro}}\cdot\tilde{W}_{ro}\right) + \varepsilon_0\right] + \dot{\zeta} \\ \le {} & \sigma'^T\left[\dot{f}_g + (c+\lambda_1)f_g + \left(\tilde{D} + 2\tilde{\Omega}\right)\ddot{q} \right. \\ & + \tilde{K}\dot{q} + (c+\lambda_1)\,\tilde{D}\dot{q} + (c+\lambda_1)\,2\tilde{\Omega}\dot{q} \\ & \left. + (c+\lambda_1)\,\tilde{K}\dot{q} - \rho\right] + \|\sigma'\|\left[\tilde{W}^T\hat{l} \right. \\ & \left. + \hat{W}^T\left(l_c\cdot\tilde{c} + l_b\cdot\tilde{b} + l_r\cdot\tilde{r} + l_{W_{ro}}\cdot\tilde{W}_{ro}\right) + \varepsilon_0\right] + \dot{\zeta} \\ = {} & \sigma'^T\left[\dot{f}_g + (c+\lambda_1)f_g - \rho\right] \\ & + \|\sigma'\|\left[\tilde{W}^T\hat{l} + \hat{W}^T\left(l_c\cdot\tilde{c} + l_b\cdot\tilde{b} \right.\right. \\ & \left.\left. + l_r\cdot\tilde{r} + l_{W_{ro}}\cdot\tilde{W}_{ro}\right) + \varepsilon_0\right] + \sigma'^T\left[\tilde{D}\ddot{q} + (c+\lambda_1)\,\tilde{D}\dot{q}\right] \\ & + tr\left\{\tilde{D}M^{-1}\dot{\tilde{D}}^T\right\} + 2\sigma'^T\left[\tilde{\Omega}\ddot{q} + (c+\lambda_1)\,\tilde{\Omega}\dot{q}\right] \\ & + tr\left\{\tilde{\Omega}N^{-1}\dot{\tilde{\Omega}}^T\right\} + \sigma'^T\left[\tilde{K}\dot{q} + (c+\lambda_1)\,\tilde{K}q\right] \\ & + tr\left\{\tilde{K}P^{-1}\dot{\tilde{K}}^T\right\} + \frac{1}{\eta_1}\dot{\tilde{W}}^T\tilde{W} \\ & + \frac{1}{\eta_2}\dot{\tilde{c}}^T\tilde{c} + \frac{1}{\eta_3}\dot{\tilde{b}}^T\tilde{b} + \frac{1}{\eta_4}\dot{\tilde{r}}^T\tilde{r} + \frac{1}{\eta_5}\dot{\tilde{W}}_{ro}^T\tilde{W}_{ro} \end{aligned} \tag{34}$$

Let:

$$\begin{aligned} & tr\left\{\tilde{D}\left[M^{-1}\dot{\tilde{D}}^T + \ddot{q}\sigma'^T + (c+\lambda_1)\,\dot{q}\sigma'^T\right]\right\} = 0, \\ & tr\left\{\tilde{K}\left[N^{-1}\dot{\tilde{K}}^T + \dot{q}\sigma'^T + (c+\lambda_1)\,q\sigma'^T\right]\right\} = 0, \\ & tr\left\{\tilde{\Omega}\left[P^{-1}\dot{\tilde{\Omega}}^T + 2\ddot{q}\sigma'^T + 2\,(c+\lambda_1)\,\dot{q}\sigma'^T\right]\right\} = 0, \\ & \|\sigma'\|\,\tilde{W}^T\hat{l} + \frac{1}{\eta_1}\dot{\tilde{W}}^T\tilde{W} = 0, \|\sigma'\|\,\hat{W}^T l_c\tilde{c} + \frac{1}{\eta_2}\dot{\tilde{c}}^T\tilde{c} = 0, \\ & \|\sigma'\|\,\hat{W}^T l_b\tilde{b} + \frac{1}{\eta_3}\dot{\tilde{b}}^T\tilde{b} = 0, \|\sigma'\|\,\hat{W}^T l_r\tilde{r} + \frac{1}{\eta_4}\dot{\tilde{r}}^T\tilde{r} = 0, \\ & \|\sigma'\|\,\hat{W}^T l_{W_{ro}}\tilde{W}_{ro} + \frac{1}{\eta_5}\dot{\tilde{W}}_{ro}^T\tilde{W}_{ro} = 0 \end{aligned} \tag{35}$$

When (35) is established, $\dot{V}_2 \leq 0$ can be satisfied, and the adaptive laws of $\hat{D}$, $\hat{K}$, $\hat{\Omega}$, $\hat{W}$, $\hat{c}$, $\hat{b}$, $\hat{r}$, $\hat{W}_{ro}$ can be obtained as:

$$\begin{aligned}
\dot{\hat{D}}^T &= -M\left[\ddot{q}\sigma'^T + (c+\lambda_1)\,\dot{q}\sigma'^T\right] \\
\dot{\hat{K}}^T &= -N\left[\dot{q}\sigma'^T + (c+\lambda_1)\,q\sigma'^T\right] \\
\dot{\hat{\Omega}}^T &= -2P\left[\ddot{q}\sigma'^T + (c+\lambda_1)\,\dot{q}\sigma'^T\right] \\
\dot{\hat{W}} &= -\eta_1 \left\|\sigma'\right\| \hat{l} \\
\dot{\hat{c}}^T &= -\eta_2 \left\|\sigma'\right\| \hat{W}^T l_c \\
\dot{\hat{b}}^T &= -\eta_3 \left\|\sigma'\right\| \hat{W}^T l_b \\
\dot{\hat{r}}^T &= -\eta_4 \left\|\sigma'\right\| \hat{W}^T l_r \\
\dot{\hat{W}}_{ro}^T &= -\eta_5 \left\|\sigma'\right\| \hat{W}^T l_{W_{ro}}
\end{aligned} \tag{36}$$

Substituting (36) into (34) obtains:

$$\begin{aligned}
\dot{V}_2 &\leq \sigma'^T\left[\dot{f}_g + (c+\lambda_1) f_g - \rho\right] + \left\|\sigma'\right\|\left[\hat{W}^T\cdot\Delta + \varepsilon_0\right] \\
&\leq \left\|\sigma'\right\|\left\|\dot{f}_g + (c+\lambda_1) f_g - \rho\right\| + \varepsilon_0\left\|\sigma'\right\| \\
&\leq \left\|\sigma'\right\|\left\|F_{d_2} + (c+\lambda_1) F_{d_1} - \rho\right\| + \varepsilon_0\left\|\sigma'\right\|
\end{aligned} \tag{37}$$

Because $\left\|F_{d_2} + (c+\lambda_1) F_{d_1}\right\| \leq \hat{\rho}$, so $\|F_{d_2} + (c+\lambda_1) F_{d_1} - \rho\| \leq -\varepsilon_0$, that is, $\dot{V}_2 \leq 0$ is guaranteed, which is negative semidefinite, that is, the system tracking track can reach the designed fractional sliding surface and remain on the sliding surface. Integrating inequality $\dot{V}_2 \leq -\left\|\sigma'\right\|\left(\|\rho\| - \left\|F_{d_2} + (c+\lambda_1) F_{d_1}\right\| - \|\varepsilon_0\|\right)$, we can get $\int_0^t \left\|\sigma'\right\| dt \leq \frac{1}{\|\rho\| - \left\|F_{d_2} + (c+\lambda_1) F_{d_1}\right\| - \|\varepsilon_0\|}\left[V_2(t) - V_2(0)\right]$. Because $V_2(t)$ is nonincreasing, and $V_2(0)$, $V_2(t)$ are bounded, we can know that $\int_0^t \|\sigma'\|(\|\rho\| - \|F_{d_2} + (c+\lambda_1) F_{d_1}\| - \|\varepsilon_0\|)dt$ is bounded.

Barbalat's Lemma: Suppose $f(t) \in C^1(a,\infty)$ and $\lim_{t\to\infty} f(t) = \alpha$ where $\alpha < \infty$. If f' is uniformly continuous, then $\lim_{t\to\infty} f'(t) = 0$.

According to Barbalat's Lemma and its deductions, the system is asymptotically stable. In addition, the tracking error and fractional sliding surface converge to zero asymptotically.

VI. SIMULATION RESULTS

MATLAB/Simulink is used to simulate the proposed method. The adaptive sliding mode control method and the fractional sliding mode control method are compared with the proposed method.

The parameters in the micro gyroscope system are set as:

$$\begin{aligned}
&m = 1.8\times10^{-7}kg, \quad d_{xx} = 1.8\times10^{-6}N\cdot s/m, \\
&d_{xy} = 3.6\times10^{-7}N\cdot s/m, \quad d_{yy} = 1.8\times10^{-6}N\cdot s/m, \\
&k_{xx} = 63.955N/m, \quad k_{xy} = 12.779N/m, \\
&k_{yy} = 95.92N/m, \quad \Omega_z = 100rad/s, q_0 = 1\mu m, \\
&\omega_0 = 1kHz.
\end{aligned}$$

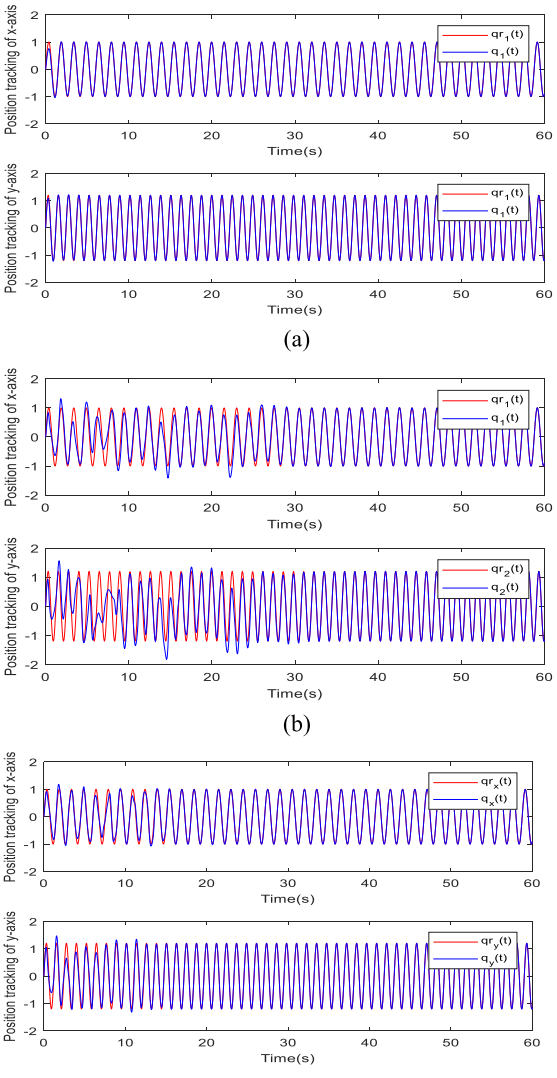

FIGURE 4. Trajectory tracking. (a) Proposed controller. (b) Adaptive sliding mode controller. (c) Fractional sliding mode controller.

Consequently, the infinite rigidification parameters of the micro gyroscope in (5) are:

$$\begin{aligned}
&d_{xx} = 0.01, \quad d_{xy} = 0.002, \; d_{yy} = 0.01, \; \omega_x^2 = 355.3, \\
&\omega_{xy} = 70.99, \quad \omega_y^2 = 532.9, \; \Omega_z = 0.1.
\end{aligned}$$

In the simulation study, the initial conditions of the system are set as: $q_1(0) = 0$, $\dot{q}_1(0) = 2.5$, $q_2(0) = 0$, $\dot{q}_2(0) = 5.5$. The expected trajectories of the micro gyroscope are set as: $q_{r1} = \sin(4.17t)$, $q_{r2} = 1.2\sin(5.11t)$. The parameters of the dynamic fractional order sliding mode switching function are set as: $c = 3$, $\lambda_1 = 2$, $\lambda_2 = 50$, The order was set to 0.1, 0.2, 0.6, 0.85, 0.95, and the root mean square error was compared, as shown in Table 1, to determine the order $\alpha = 0.85$ of the fractional order. The adaptive fixed gain is set to: $M = diag(5,5)$, $N = diag(10,10)$, $P = diag(1,1)$. The estimated initial values of the three parameter matrices are set as: $\hat{D}(0) = 0.95 * D$, $\hat{K}(0) = 0.95 * K$, $\hat{\Omega}(0) = 0$. The parameters in the double feedback fuzzy neural network

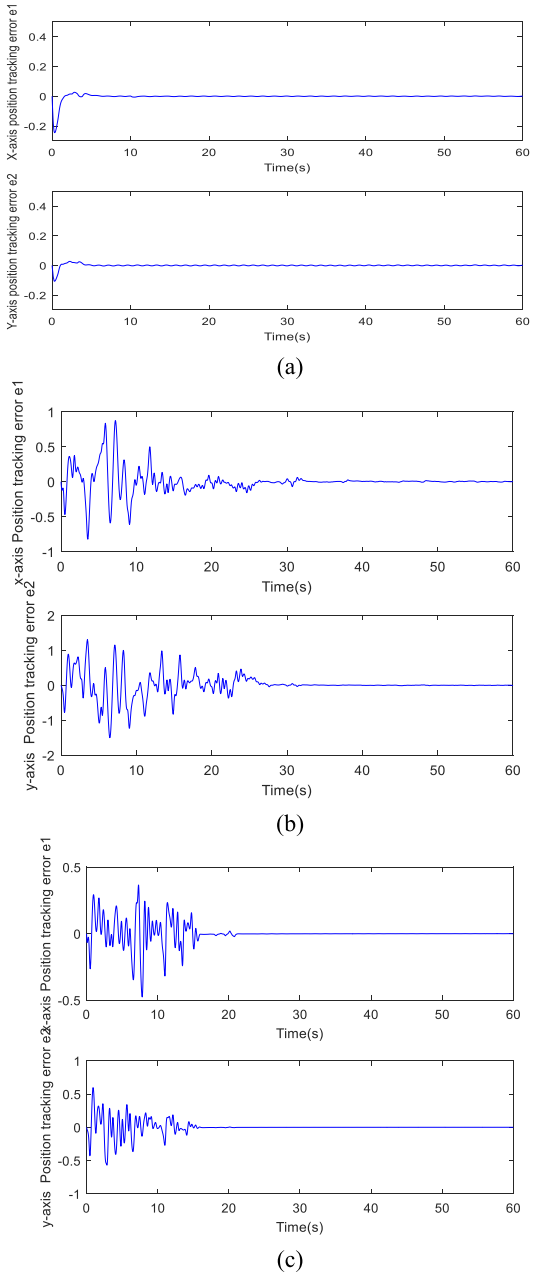

FIGURE 5. Tracking error. (a) Proposed controller. (b) Adaptive sliding mode controller. (c) Fractional sliding mode controller.

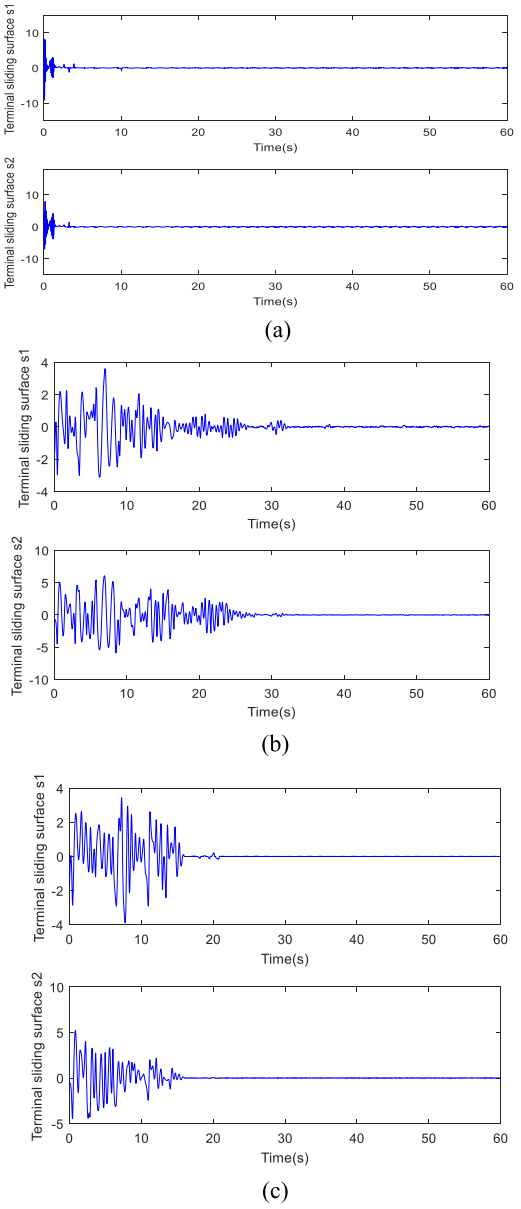

FIGURE 6. Convergence of sliding mode surfaces. (a) Proposed controller. (b) Adaptive sliding mode controller. (c) Fractional sliding mode controller.

structure are set: $k = 2, i = 5, m = 5$. Namely, the initial values of base width, weight, center vector, outer layer gain and inner layer gain of neural network are respectively taken as:

$$b = \begin{bmatrix} 1 & 1 & 1 & 1 & 1 \\ 1 & 1 & 1 & 1 & 1 \end{bmatrix},$$

$$W = \begin{bmatrix} -1.6 & -0.01 & -0.01 & -0.1 & -0.1 \\ -1.6 & -0.01 & -0.01 & -0.1 & -0.1 \end{bmatrix},$$

$$c = \begin{bmatrix} -2.5 & -1.25 & 0 & 1.25 & 2.5 \\ -2.5 & -1.25 & 0 & 1.25 & 2.5 \end{bmatrix}, W_{ro} = \begin{bmatrix} 20 \\ 20 \end{bmatrix},$$

$$W_r = \begin{bmatrix} -0.2 & -0.5 & 0 & 0.05 & 0.3 \\ -0.2 & -0.5 & 0 & 0.05 & 0.3 \end{bmatrix}.$$

TABLE 1. RMSE of different orders.

Order α	RMSE of x-axis tracking error	RMSE of y-axis tracking error
0.1	0.0286	0.0234
0.2	0.0256	0.0146
0.6	0.0249	0.0126
0.85	0.0240	0.0107
0.95	0.0241	0.0114

The adaptive law gains of neural network are taken as: $\eta_1 = 10$, $\eta_2 = 15000$, $\eta_3 = 1$, $\eta_4 = 0.001$, $\eta_5 = 0.5$. The random signal is taken as: $d = [randn\,(1, 1)\,; randn\,(1, 1)]$.

The simulation time is set to 60s. Fig. 4(a) shows that the tracking properties obtained by using the

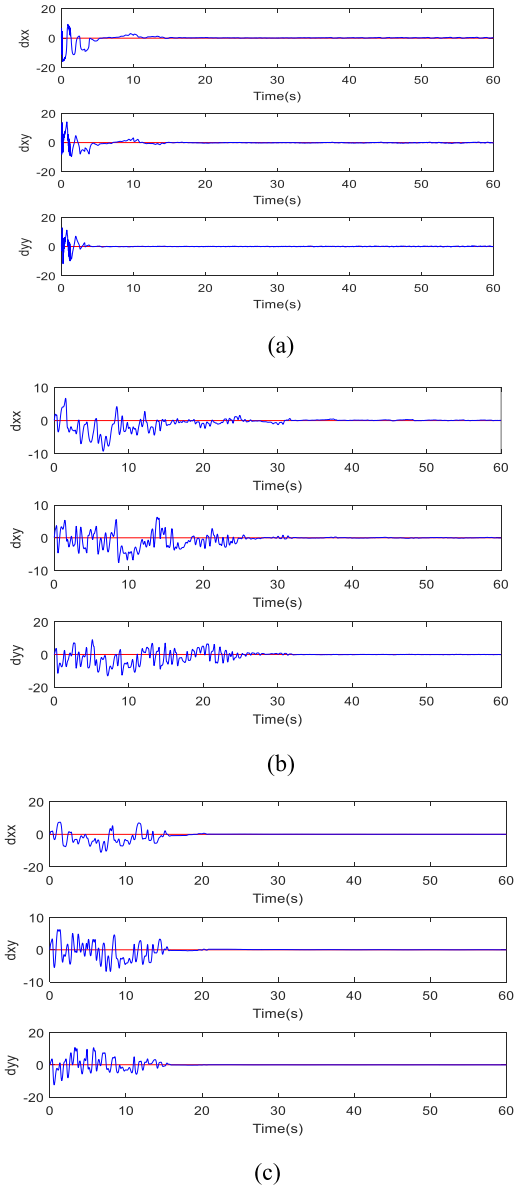

FIGURE 7. d_{xx}, d_{xy}, d_{yy} adaptive identification curve. (a) Proposed controller. (b) Adaptive sliding mode controller. (c) Fractional sliding mode controller.

TABLE 2. RMSE of different methods.

Method	RMSE of x-axis tracking error	RMSE of y-axis tracking error
Proposed controller	0.0286	0.0107
Adaptive fractional sliding mode controller	0.0721	0.0932

proposed dynamic fractional order sliding mode controller. Fig.4(b) and (c) shows the tracking curves obtained by using ordinary adaptive sliding mode controller and fractional

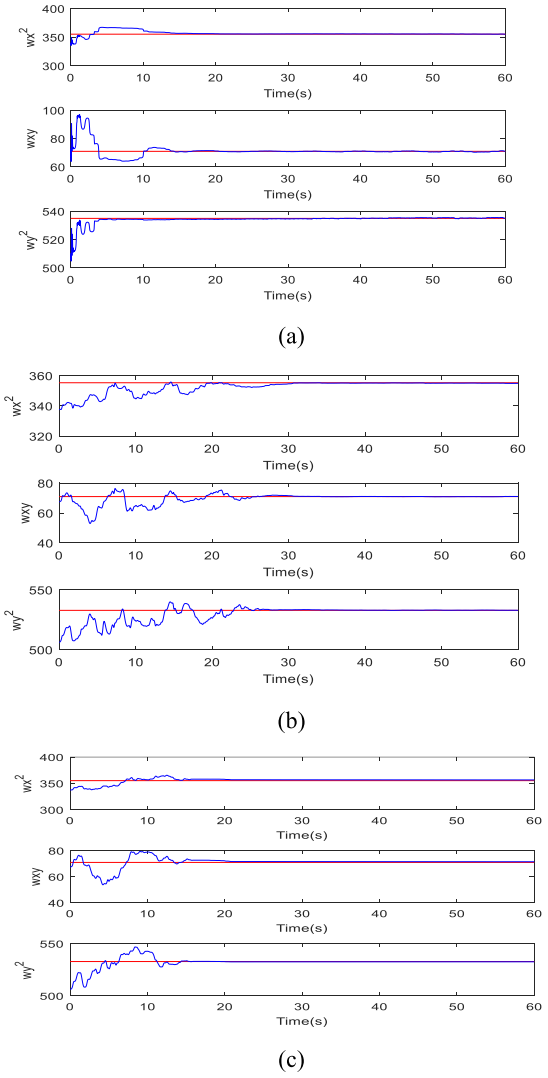

FIGURE 8. ω_x^2, ω_{xy}, ω_y^2 adaptive identification curve. (a) Proposed controller. (b) Adaptive sliding mode controller. (c) Fractional sliding mode controller.

sliding mode controller. Fig. 5 shows the tracking error of the system. The root mean square errors of the proposed methods are $RMSE_x = 0.0240$ and $RMSE_y = 0.0107$, the $RMSE_x = 0.1690$ and $RMSE_y = 0.3230$ for ordinary sliding mode control, and the $RMSE_x = 0.0721$ and $RMSE_y = 0.0932$ for fractional sliding mode control. Compared with the tracking error and root mean square errors of tracking error, the tracking error of the proposed dynamic fractional sliding mode control system can converge to zero better and track the reference track faster in a limited time. Fig. 6 shows the convergence of the sliding surface using the three control methods. The switching functions of the three control methods are different. The proposed method in this paper can effectively reduce the chattering, and the convergence speed of the system is high. The control system can reach the sliding surface in a short time. Fig.7, Fig. 8 and Fig. 9 are adaptive identification curves for unknown parameters of the micro gyroscope system. In these three cases, the unknown

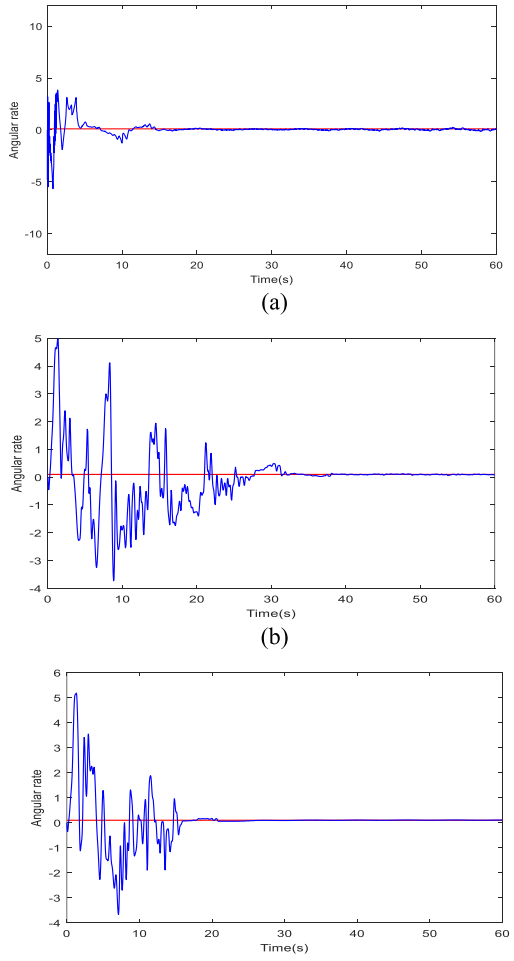

FIGURE 9. Ω_z adaptive identification curve. (a) Proposed controller. (b) Adaptive sliding mode controller. (c) Fractional sliding mode controller.

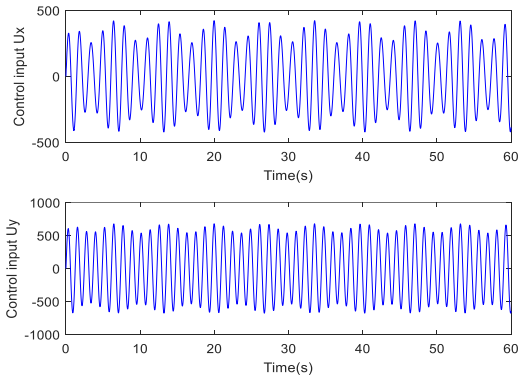

FIGURE 10. Control input of x-axis and y-axis using proposed controller.

parameters can converge near their true values. However, the proposed neural network dynamic sliding mode control law has faster convergence speed and better performance. The adaptive identification curves of the base width, the center vector, the weight of the output layer, the inner gain and the outer gain of the double feedback fuzzy network are shown in Figs. 11-15 respectively. The parameters of the fuzzy network can basically approach stable values.

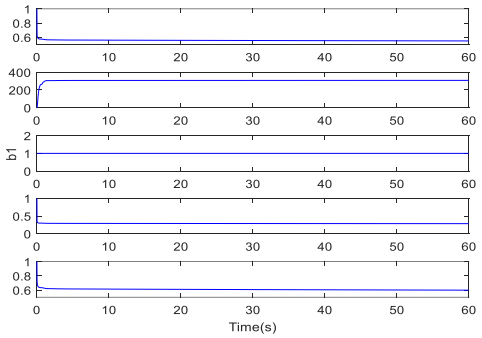

FIGURE 11. Base width b_1 adaptive identification.

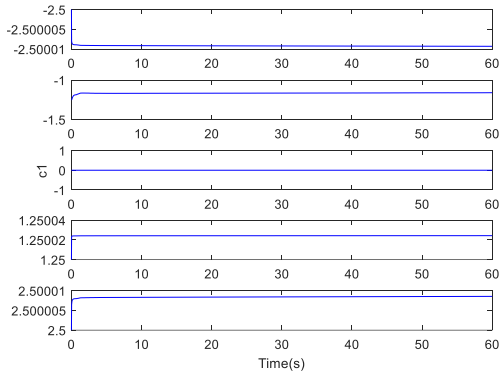

FIGURE 12. Center vector c_1 adaptive identification.

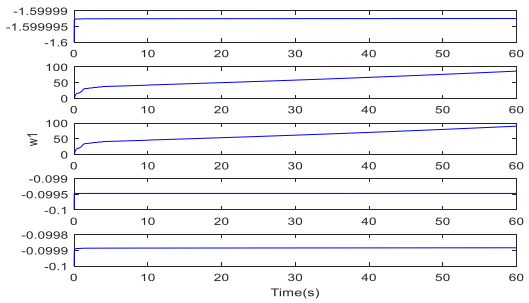

FIGURE 13. Weight W adaptive identification of output layer neural network.

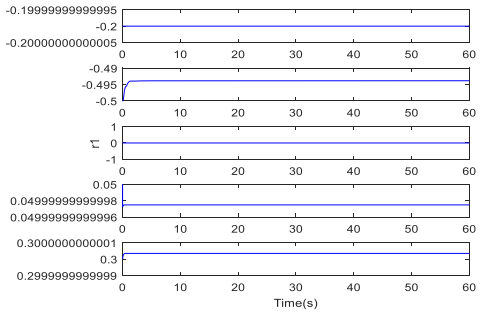

FIGURE 14. Inner gain r_1 adaptive identification.

The method proposed in this paper is different from the method in [6], compared with the method in [6], the method proposed in this paper can approach the unknown parameters of the system faster and reduce the chattering with better performance as shown in Table 2.

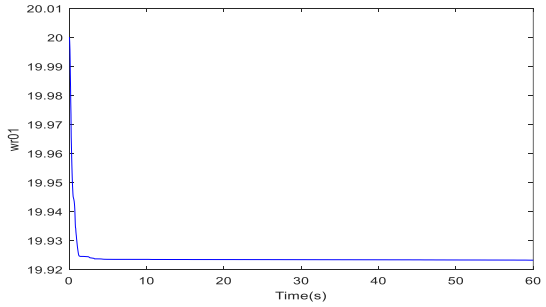

FIGURE 15. Outer gain W_{ro} adaptive identification.

VII. CONCLUSION

A dynamic fractional order sliding mode control method based on a double feedback fuzzy neural network is presented. A fuzzy neural network controller with double feedback mechanism is used to approximate the lumped uncertainty, and the estimated value is used to replace its true value as the gain of the switching control law. The switching function of dynamic fractional sliding mode control can reduce the chattering, provide the higher degree of freedom, and improve the convergence speed. Moreover, Lyapunov stability theory can update the estimates of the system unknown parameters in real time. The simulation results show that, compared with the ordinary adaptive sliding mode control method and fractional sliding mode controller, the proposed control method improves the control accuracy and the convergence speed, reduces the output signal tracking error, thereby verifying the effectiveness and feasibility of the proposed method.

REFERENCES

[1] C. Jia and B. L. Evans, "Online camera-gyroscope autocalibration for cell phones," *IEEE Trans. Image Process.*, vol. 23, no. 12, pp. 5070–5081, Dec. 2014.
[2] D. Xia, Y. Hu, and P. Ni, "A digitalized gyroscope system based on a modified adaptive control method," *Sensors*, vol. 16, no. 3, p. 321, Mar. 2016.
[3] M. H. Choi, B. Shirinzadeh, and R. Porter, "System identification-based sliding mode control for small-scaled autonomous aerial vehicles with unknown aerodynamics derivatives," *IEEE/ASME Trans. Mechatronics*, vol. 21, no. 6, pp. 2944–2952, Dec. 2016.
[4] J. Song, Y. Niu, and Y. Zou, "A parameter-dependent sliding mode approach for finite-time bounded control of uncertain stochastic systems with randomly varying actuator faults and its application to a parallel active suspension system," *IEEE Trans. Ind. Electron.*, vol. 65, no. 10, pp. 8124–8132, Oct. 2018.
[5] J. Fei and Z. Feng, "Adaptive fuzzy super-twisting sliding mode control for microgyroscope," *Complexity*, vol. 2019, pp. 1–13, Feb. 2019.
[6] F. Chen and J. Fei, "Fractional order adaptive sliding mode control system of micro gyroscope," *IEEE Access*, vol. 7, pp. 150565–150572, 2019.
[7] G. Costantini, D. Casali, and R. Perfetti, "Associative memory design for 256 gray-level images using a multilayer neural network," *IEEE Trans. Neural Netw.*, vol. 17, no. 2, pp. 519–522, Mar. 2006.
[8] Z. Yun, Z. Quan, S. Caixin, L. Shaolan, L. Yuming, and S. Yang, "RBF neural network and ANFIS-based short-term load forecasting approach in real-time price environment," *IEEE Trans. Power Syst.*, vol. 23, no. 3, pp. 853–858, Aug. 2008.
[9] M. E. Karar, "Robust RBF neural network-based backstepping controller for implantable cardiac pacemakers," *Int. J. Adapt. Control Signal Process.*, vol. 32, no. 7, pp. 1040–1051, Apr. 2018.
[10] C. A. Perez, C. A. Salinas, P. A. Estevez, and P. M. Valenzuela, "Genetic design of biologically inspired receptive fields for neural pattern recognition," *IEEE Trans. Syst., Man Cybern., Part B*, vol. 33, no. 2, pp. 258–270, Apr. 2003.
[11] H.-J. Yang and M. Tan, "Sliding mode control for flexible-link manipulators based on adaptive neural networks," *Int. J. Autom. Comput.*, vol. 15, no. 2, pp. 239–248, Apr. 2018.
[12] Y. Saeed, K. Ahmed, M. Zareei, A. Zeb, C. Vargas-Rosales, and K. M. Awan, "In-vehicle cognitive route decision using fuzzy modeling and artificial neural network," *IEEE Access*, vol. 7, pp. 20262–20272, 2019.
[13] D. Qian and G. Fan, "Neural-network-based terminal sliding mode control for frequency stabilization of renewable power systems," *IEEE/CAA J. Automatica Sinica*, vol. 5, no. 3, pp. 706–717, May 2018.
[14] G. Qiao and C. Peng, "Backstepping sliding mode control with self recurrent wavelet neural network observer for a novel coaxial twelve-rotor UAV," *High Technol. Lett.*, vol. 24, no. 2, pp. 142–148, 2018.
[15] Y. Chu, J. Fei, and S. Hou, "Adaptive global sliding-mode control for dynamic systems using double hidden layer recurrent neural network structure," *IEEE Trans. Neural Netw. Learn. Syst.*, vol. 31, no. 4, pp. 1297–1309, Apr. 2020, doi: 10.1109/TNNLS.2019.2919676.
[16] J. Fei and Y. Chu, "Double hidden layer output feedback neural adaptive global sliding mode control of active power filter," *IEEE Trans. Power Electron.*, vol. 35, no. 3, pp. 3069–3084, Mar. 2020.
[17] J. Fei and H. Wang, "Experimental investigation of recurrent neural network fractional-order sliding mode control of active power filter," *IEEE Trans. Circuits Syst. II, Exp. Briefs*, early access, Nov. 12, 2019, doi: 10.1109/TCSII.2019.2953223.
[18] S. Hou and J. Fei, "A self-organizing global sliding mode control and its application to active power filter," *IEEE Trans. Power Electron.*, vol. 35, no. 7, pp. 7640–7652, Jul. 2020, doi: 10.1109/TPEL.2019.2958051.
[19] Y. Yin, J. Liu, J. A. Sanchez, L. Wu, S. Vazquez, J. I. Leon, and L. G. Franquelo, "Observer-based adaptive sliding mode control of NPC converters: An RBF neural network approach," *IEEE Trans. Power Electron.*, vol. 34, no. 4, pp. 3831–3841, Apr. 2019.
[20] N. Fethalla, M. Saad, H. Michalska, and J. Ghommam, "Robust observer-based dynamic sliding mode controller for a quadrotor UAV," *IEEE Access*, vol. 6, pp. 45846–45859, 2018.
[21] Y. Chen and J. Fei, "Dynamic sliding mode control of active power filter with integral switching gain," *IEEE Access*, vol. 7, pp. 21635–21644, 2019.
[22] J. Fei and Y. Chen, "Dynamic terminal sliding-mode control for single-phase active power filter using new feedback recurrent neural network," *IEEE Trans. Power Electron.*, vol. 35, no. 9, pp. 9906–9924, Sep. 2020.
[23] F.-J. Lin, Y.-C. Hung, and S.-Y. Chen, "Field-programmable gate array-based intelligent dynamic sliding-mode control using recurrent wavelet neural network for linear ultrasonic motor," *IET Control Theory Appl.*, vol. 4, no. 9, pp. 1511–1532, Sep. 2010.
[24] S. Xu, G. Sun, Z. Ma, and X. Li, "Fractional-order fuzzy sliding mode control for the deployment of tethered satellite system under input saturation," *IEEE Trans. Aerosp. Electron. Syst.*, vol. 55, no. 2, pp. 747–756, Apr. 2019.
[25] P. Mani, R. Rajan, L. Shanmugam, and Y. H. Joo, "Adaptive fractional fuzzy integral sliding mode control for PMSM model," *IEEE Trans. Fuzzy Syst.*, vol. 27, no. 8, pp. 1674–1686, Aug. 2019.
[26] Y. Fang, J. Fei, and D. Cao, "Adaptive fuzzy-neural fractional-order current control of active power filter with finite-time sliding controller," *Int. J. Fuzzy Syst.*, vol. 21, no. 5, pp. 1533–1543, Jul. 2019.
[27] J. Fei and X. Liang, "Adaptive backstepping fuzzy neural network fractional-order control of microgyroscope using a nonsingular terminal sliding mode controller," *Complexity*, vol. 2018, pp. 1–12, Sep. 2018, doi: 10.1155/2018/5246074.
[28] J. Fei and Z. Feng, "Fractional-order finite-time super-twisting sliding mode control of micro gyroscope based on double-loop fuzzy neural network," *IEEE Trans. Syst., Man, Cybern. Syst.*, early access, Mar. 25, 2020, doi: 10.1109/TSMC.2020.2979979.
[29] M. P. Aghababa, "A novel terminal sliding mode controller for a class of non-autonomous fractional-order systems," *Nonlinear Dyn.*, vol. 73, nos. 1–2, pp. 1–10, 2013.
[30] Y. Li, Y. Chen, and I. Podlubny, "Stability of fractional-order nonlinear dynamic systems: Lyapunov direct method and generalized Mittag–Leffler stability," *Comput. Math. Appl.*, vol. 59, no. 5, pp. 1810–1821, Mar. 2010.

JUNTAO FEI (Senior Member, IEEE) received the B.S. degree in electrical engineering from the Hefei University of Technology, China, in 1991, the M.S. degree in electrical engineering from the University of Science and Technology of China, in 1998, and the M.S. and Ph.D. degrees in mechanical engineering from The University of Akron, OH, USA, in 2003 and 2007, respectively. He was a Visiting Scholar with the University of Virginia, VA, USA, from 2002 to 2003. He was a Postdoctoral Research Fellow and an Assistant Professor with the University of Louisiana, LA, USA, from 2007 to 2009. He is currently a Professor with Hohai University, China. His research interests include adaptive control, nonlinear control, intelligent control, dynamics and control of MEMS, and smart materials and structures.

FANG CHEN received the B.S. degree in electrical engineering from Henan University, China, in 2018. She is currently pursuing the M.S. degree in electrical engineering with Hohai University, China. Her research interests include adaptive control, power electronics, nonlinear control, and neural networks.